JMEPEG (2010) 19:880–884
DOI: 10.1007/s11665-009-9544-1

1059-9495/$19.00

Effect of Boron Additions on Sintering and Densification of a Ferritic Stainless Steel

J.A. Cabral Miramontes, J.D.O. Barceinas Sánchez, F. Almeraya Calderón, A. Martínez Villafañe, and J.G. Chacón Nava

(Submitted June 23, 2008; in revised form July 21, 2009)

The effect of boron additions on the densification of a ferritic stainless steel during sintering was studied. Experimental results showed that density and microstructure changed with the boron content. Boron promotes the formation of a liquid phase, which resulted from a eutectic reaction involving iron and chromium. The presence of the liquid phase modified the microstructure morphology, shape of porosity, density, and hardness.

Keywords 409Nb stainless steel, densification, DTA, hardness, liquid phase sintering

1. Introduction

The main attraction of powder metallurgy (PM) is its ability to manufacture large quantities of high-quality structural and engineering parts, which are greatly valued due to their properties, i.e., acceptable corrosion resistance, good appearance, and satisfactory physical and mechanical properties for their intended applications. Some additional advantages are: low processing temperature, more efficient energy and material usage (scrap is lower than 5%), and more homogeneous and refined microstructures (Ref 1, 2).

Sintering stainless steel is difficult due to the presence of a thin chromium oxide layer that covers the powder particles. This layer slows down atomic diffusion between particles resulting in both low densities and poor mechanical properties. To overcome this drawback, the utilization of a hydrogen base atmosphere is mandatory to reduce this oxide (Ref 3). Since the melting point of ferritic stainless steels is higher than that of carbon or low-alloy steels, the recommended sintering temperature can be very high (up to ~1360 °C). One strategy to diminish this temperature can be the activation of the sintering process by adding boron (Ref 4-7). This promotes the formation of a liquid phase by the occurrence of a eutectic reaction (Ref 8). Boron seems to be the ideal additive for improving the sintering of iron-based alloys (Ref 4). The binary Fe-B phase diagram shows the presence of an intermetallic Fe_2B, which forms a eutectic compound with iron at 1174 °C and 4 wt.% B (Ref 9). When the boron content is increased, the amount of eutectic (liquid) increases, which results in high densities, rounded pores, and improved mechanical properties (Ref 4, 8).

Reports on the effect of adding boron to low-alloy steels, austenitic stainless steels, duplex-type steels, and martensitic stainless steel can be found in the literature (Ref 10-12). However, there is no information about the effect of boron on ferritic stainless steels produced by powder metallurgy. Thus, the objective of this investigation was to study the effect of the boron content on the densification and microstructure of a 409Nb/Fe-B/Fe-Cr alloy on sintering.

2. Experimental Procedure

409Nb (Coldstream, Ath, Belgium) stainless steel, iron-chromium (Fe-Cr), and iron-boron (Fe-B) (F. W. Winter & Co., Camden, NJ) powders were used as base materials. Chemical composition and physical properties of the powders are shown in Table 1. Three mixtures were prepared in which the boron content was varied from 0.8, 0.9, and 1.2 wt.%. 2.6 wt.% Fe-Cr was added to all mixtures; a sample without boron addition was prepared as reference (Fe0.0B). The chemical composition and nomenclature of the mixtures are shown in Table 2.

The mixtures were blended in a double-cone mixer spinning at 20 rpm for 30 min. 1 wt.% Zinc stearate (Blachford) was added as lubricant to all mixtures.

Cylindrical specimens of 9.5 mm length and 10.2 mm diameter were compacted at 700 MPa using a closed-end die. Sintering was carried out in a horizontal tubular furnace at 1150 °C for 60 min under a hydrogen atmosphere and heating at 20°C/min. Green density was determined by measuring weight and volume, while the density of the sintered specimens was obtained by Archimedes method (Ref 13). Both relative green density and relative sintered density were calculated by employing the rule of mixtures.

Small fragments of compacted specimens were subjected to differential thermal analysis (DTA) in a simultaneous TGA/DSC analyzer model SDT Q600 from TA Instruments, under an argon atmosphere and heating at 20°C/min up to 1300 °C.

Sintered samples were cut, mounted, and metallographically prepared for analysis in a scanning electron microscope JEOL

J.A. Cabral Miramontes, F. Almeraya Calderón, A. Martínez Villafañe, and **J.G. Chacón Nava**, Centro de Investigación en Materiales Avanzados S.C., Miguel de Cervantes Saavedra 120, C.P. 31104 Chihuahua, CH, Mexico; and **J.D.O. Barceinas Sánchez**, Centro de Investigación en Ciencia Aplicada y Tecnología Avanzada del I.P.N., Cerro Blanco 141, C.P. 76090 Querétaro, QE, Mexico. Contact e-mail: jose.chacon@cimav.edu.mx.

Table 1 Chemical composition (wt.%) and powder properties

Powder	Composition (wt.%)*							Apparent density*, g/cm^3	Flow*, s/50g
	Fe	Cr	B	C	S	Nb	Si		
409Nb	87.52	10.90	···	0.01	0.01	0.53	0.90	3.06	26.20
Fe-Cr	24.93	74.00	···	0.03	0.02	···	1.00	4.11	···
Fe-B	79.67	···	18.98	0.35	0.005	···	0.82	1.44	···

Powder	Granulometry* (%)						
	−60 + 80	−80 + 100	−100 + 150	−150 + 200	−200 + 250	−250 + 325	−325
409Nb	0.03	0.19	7.26	31.92	11.99	24.65	23.96
Fe-Cr	100.00	···	···	···	···	···	15.00 max
Fe-B	···	···	···	···	···	0.01	99.99

* Data provided by the manufacturer

Table 2 Chemical composition and nomenclature of mixtures

Mixture	Chemical composition (wt.%)					
	Fe	Cr	B	C	Nb	Si
Fe0.0B	Bal	13.5	0.0	0.002	0.50	0.89
Fe0.8B	Bal	13.5	0.8	0.184	0.47	0.89
Fe0.9B	Bal	13.5	0.9	0.207	0.47	0.89
Fe1.2B	Bal	13.5	1.2	0.275	0.46	0.89

Model JSM-5800LV. Rockwell B hardness measurements were carried out in a Wilson Rockwell Tester Model C503R.

X-ray diffraction analysis of sintered specimens was performed in a Siemens diffractometer, model D5000, employing Cu Kα_1 radiation (λ = 1.54184 Å), setting up the operating voltage and current at 34 kV and 28 mA, respectively, and the scanning angle range from 10 to 100°.

3. Results and Discussion

Figure 1 shows the DTA curves of all mixtures. The exothermic broad peak maximum, which appeared at about 350 °C, corresponds to the thermal decomposition of the lubricant. The endothermic broad peak observed between 720 and 950 °C in all boron-doped samples can be associated with the α-Fe $\rightarrow$ γ-Fe transformation and dissolution of boron and carbon (Ref 14); these interstitial elements expand the γ-Fe phase field (Ref 15). These samples also showed another endothermic peak at about 1150 to 1250 °C, which indicates liquid formation by eutectic reaction. The sample Fe0.0B did not show any of the endothermic peaks. Bakan et al. reported that the increase in the eutectic temperature for an austenitic 316L stainless steel doped with either elemental boron or nickel boride, compared with the 1174 °C of the eutectic Fe-Fe_2B, was attributed to the presence of substitutional elements such as chromium and molybdenum (Ref 16). The formation of a eutectic between austenite and a complex boride of the type $(Fe, Cr, Mo)_2$-B in the temperature range of 1200 to 1240 °C was observed. In this investigation, the eutectic formation between an iron phase (most probably α-Fe) and a boride of the type $(Fe, Cr)_2$-B also occurred.

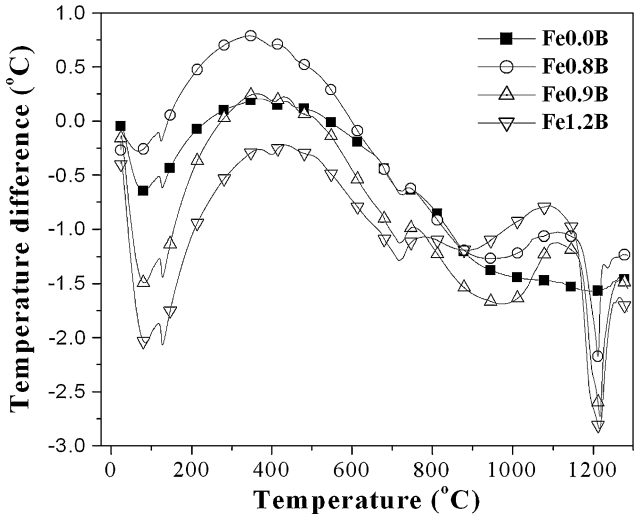

Fig. 1 DTA curves of all mixtures

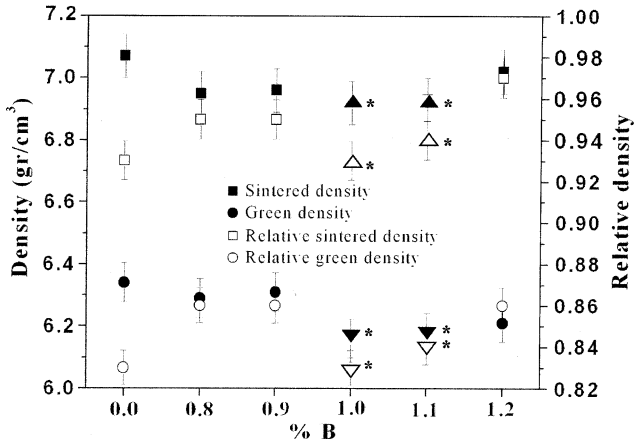

Fig. 2 Density and relative density of green and sintered samples as a function of boron content. (*) 1.0 and 1.1 wt.% boron data taken from Ref 17

Figure 2 shows the density and relative density of both green and sintered specimens as a function of boron content. The data corresponding to 1.0 and 1.1 wt.% B comes from

recent work published by the present authors (Ref 17). The green density decreased as the boron content was increased, which can be attributed to the lower density of the Fe-B powder, but the relative green density remained unchanged (~0.86) irrespective of boron content. Green density of sample Fe0.0B was higher than that of samples with boron; however, its relative green density was lower. After sintering, the reference sample density reached 7.07 g/cm^3, its relative density being 0.93. In this case, a solid-state sintering process can be assumed. The increase in density can be attributed to the reduction of the superficial oxide layer that covers the particles, resulting in enhanced contact between them, thus increasing the mass transfer. Sintered density increased as boron content was increased, but their density values were lower than that of the reference sample. Relative densities of sintered specimens also tended to increase with the boron content, but, then, were higher than that of sample Fe0.0B. Summarizing, the addition of boron increases the density when sintering at 1150 °C because of the formation of a liquid phase.

The effect of boron on mechanical properties of stainless steels has remained controversial among various researchers. For instance, some researchers report that increasing boron content increases some properties such as hardness and ultimate tensile strength (UTS) (Ref 4, 10), whereas others report the contrary, concluding that the eutectic formed is brittle, which mainly affects the ductility (Ref 18). Recently, it has been reported that a PM martensitic stainless steel reached a maximum UTS when adding 1 wt.% Fe-B and sintering at 1350 °C for 60 min (Ref 12). It was also reported that adding 1 and 1.5 wt.% Fe-B and sintering at 1300 °C, the corresponding UTS values *were* lower than those achieved at 1350 °C. This was associated with the modification of the residual porosity, which had smaller size and volume, and more rounded shape as the sintering temperature increases. Table 3 shows the effect of boron on specimen hardness. As can be seen, an increase in boron content increases the specimen hardness value.

It is known that chromium stabilizes the α-Fe phase in which the volume diffusivity of boron at 919 °C is about 300 times higher than that in γ-Fe phase. The α-Fe phase is usually unstable at sintering temperatures ranging from 1000 to 1300 °C (Ref 3). However, this phase can be stabilized at this temperature range by adding more than 12.7 wt.% chromium (Ref 3), hence the dissolution of interstitial solutes (like boron and carbon) can be improved. Besides forming some carbides (Ref 19, 20), niobium also stabilizes the α-Fe phase. Chromium also tends to form carbides. Boron forms eutectic compounds with iron and chromium, Fe-Fe_2B and Cr-Cr_2B, respectively. The former occurs at 1174 °C and 4 wt.% B, while the latter at 1630 °C and 3.1 wt.%. Theoretically, the coupling of two binary systems that has a eutectic point could lead to a ternary system having a eutectic point with a melting temperature lower than that of the binaries. Therefore, in this case, the appearance of the liquid phase could occur below 1174 °C. Based on the current findings, it can be said that a ternary eutectic began to form at 1150 °C in all samples with boron.

In other alloy systems, such as Fe-Mo-C-B, the high carbon content probably promotes densification as a result of the formation of a ternary or quaternary eutectic (Ref 18). A similar situation can be expected in the Fe-Cr-C-B alloy system of this study. Research on the Fe-B-C system indicates that the optimization of carbon and boron content will produce an adequate equilibrium between strength, ductility, and contraction (Ref 11). In a similar way, carbon contributes to densification by forming additional liquid by the reaction α-Fe + Mo_2C + Fe_3C-Liquid that occurs at 1085 °C. Furthermore, a relative sintered density of 95 to 100% can be reached by adding small quantities of boron. The existence of carbides in Fe-B powders and the formation of additional metallic carbides possibly led to ternary or quaternary reactions that form an additional liquid phase.

Figure 3 shows micrographs of (a) Fe0.0B and (b) Fe0.8B. The micrograph of the reference sample revealed acute dihedral angles and gaps between some particles, which indicate that full contact with each other did not occurred. These features are usually associated with a deficient sintering. In this case, it is not clear if the hydrogen atmosphere and sintering temperature promoted extensive oxide reduction and sufficient diffusion between particles. Figure 3(b) shows the microstructure of the

Table 3 HRB values measured in all specimens

Mixture	Hardness (Rockwell B)
Fe0.0B	54 ± 2.2
Fe0.8B	65 ± 1.4
Fe0.9B	67 ± 1.7
Fe1.2B	78 ± 1.6

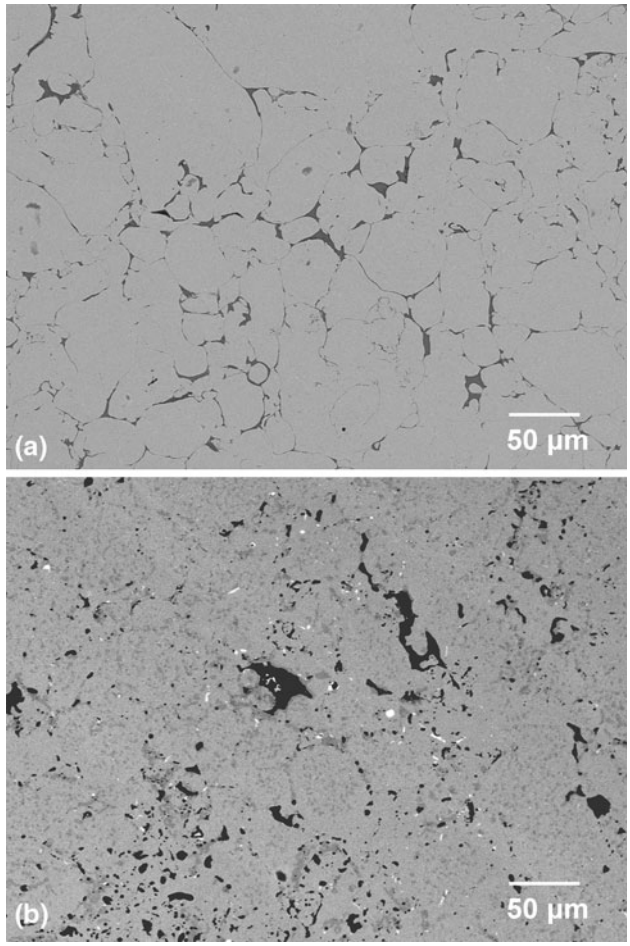

Fig. 3 Scanning electron micrographs of (a) Fe0.0B and (b) Fe0.8B sintered samples at 1150 °C for 60 min

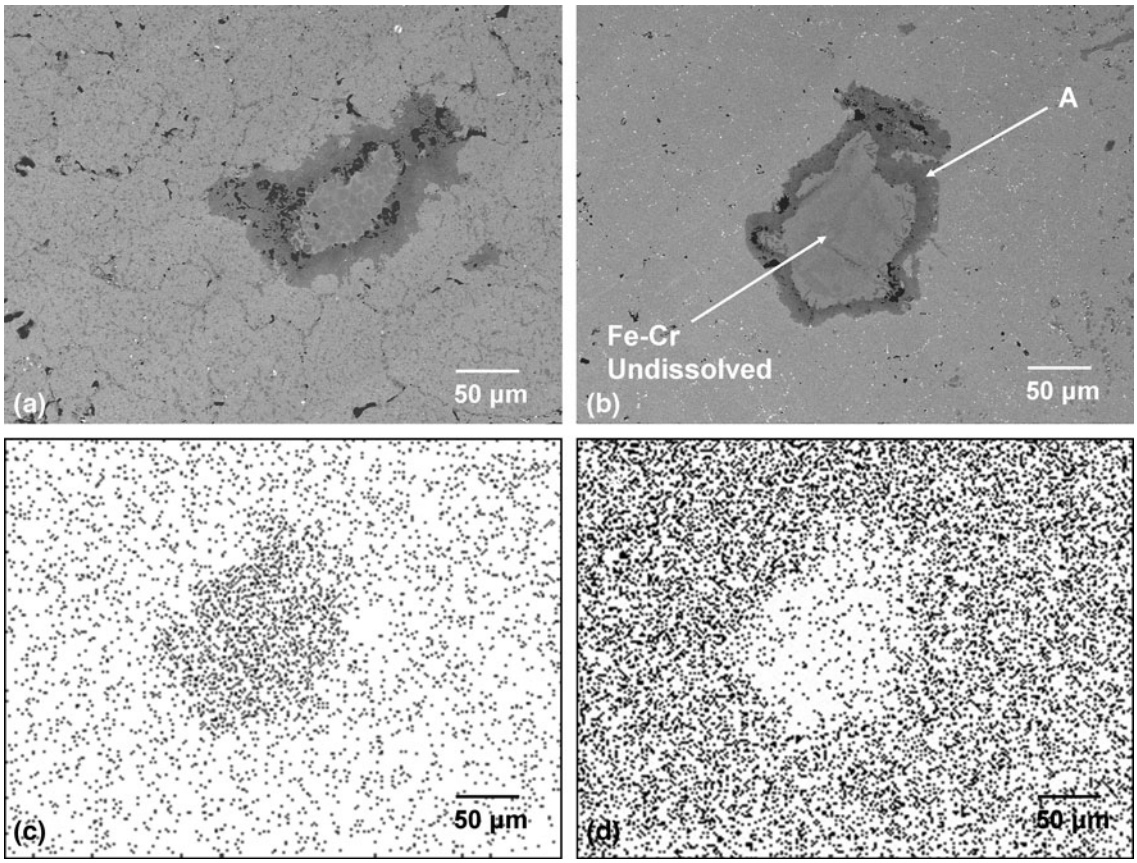

Fig. 4 Scanning electron micrographs of samples (a) Fe0.9B and (b) Fe1.2B. (c) X-ray Cr mapping for (b) and (d) x-ray Fe mapping for (b)

specimen Fe0.8B. Spherical and rounded pores at multiple point boundaries are observed. The large pores constitute secondary porosity, which resulted from the coalescence of small pores (Ref 21). Pore coalescence can be associated with the densification attained by this sample. The formation of boron compounds could also be seen. There was an increase in contact points due to the formation of these compounds; therefore, the atomic diffusion was enhanced.

Figure 4(a) shows the micrograph of the specimen Fe0.9B. Despite an obvious decrease in porosity, which cannot be seen, higher dissolution and reprecipitation of boron compounds seemed to occur. This appears to be favored by both high chromium and carbon content. In Fig. 4(b) (Fe1.2B), small and spherical pores are observed, but no grain boundaries are seen. The aforementioned finding is associated with higher densification. It seems that this sample was able to form a high quantity of liquid, which prevailed during all sintering stages. Also, reprecipitation of boron compounds seemed to occur; these compounds appear as a nonspherical dark phase (see arrow A) at some particle boundaries. In these two samples (Fig. 4a, b), small and rounded pores exist, most of them remaining isolated. Some undissolved Fe-Cr particles could also be seen. This was confirmed by chromium mapping (Fig. 4c). In addition, Fig. 4(d) shows the iron mapping acquired from the same area on Fig. 4(b).

The microstructures observed are in agreement with the density values obtained, especially for mixtures with boron. In these samples, a more homogenous microstructure without evident grain boundaries was observed. In this study, high-density values were associated with the presence of scant

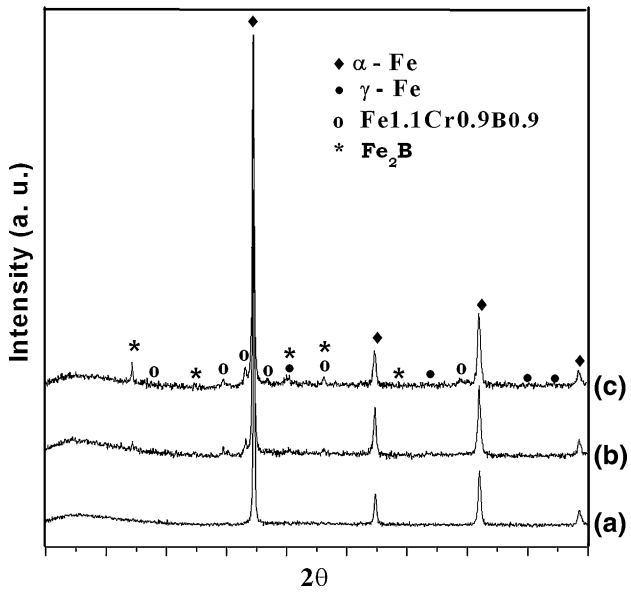

Fig. 5 Diffractograms of (a) Fe0.0B, (b) Fe0.8B, and (c) Fe1.2B sintered samples at 1150 °C for 60 min

porosity and the formation of boron compounds, which are associated with the formation of the liquid phase and improved mass transfer.

Figure 5 shows the diffractograms of the most representative samples. In all of them, the presence of the α-Fe (03-065-4899)

phase was found. This confirms that the resulting stainless steel remained ferritic. In samples with boron, the formation of small quantities of γ-Fe phase (00-052-0512), and a phase identified as Fe1.1Cr0.9B0.9 (01-072-1073) and Fe_2B (01-089-1993) were also present. This confirms that a ternary eutectic formed during sintering.

4. Conclusions

The addition of boron improves the sintering and densification of the 409Nb stainless steel during sintering at 1150 °C due to the formation of a liquid phase. Density increased accordingly with the increase in boron content. A ternary eutectic began to form at a temperature as low as 1150 °C. This was confirmed by DTA and x-ray diffraction. It was also confirmed that the resulting material remained ferritic. A maximum hardness of 78 HRB was achieved with 1.2 wt.% B. The hardness of sintered samples increased as boron content was increased. The use of a reducing atmosphere promoted solid-state sintering of the reference sample; nonetheless, the microstructural features observed are evidence of a deficient sintering.

Acknowledgment

The authors wish to thank the National Council of Science and Technology (CONACyT, Mexico) for financial support to carry out this investigation.

References

1. W. Schatt and K.P. Wieters, *Powder Metallurgy Processing and Materials*, EPMA, Shrewsbury, UK, 1997, p 47–59
2. S.S. Panda, V. Singh, A. Upadhyaya, and D. Agrawal, Sintering Response of Austenitic (316L) and Ferritic (434L) Stainless Steel Consolidated in Conventional and Microwave Furnace, *Scripta Mater.*, 2006, **54**, p 2179–2183
3. "Powder Metal Technologies and Applications," *ASM Metals Handbook*, 10th ed., ASTM B18-94, Standard, 7, American Society for Metals, 1998, p 1325–1348
4. M. Seleká, A. Šalak, and H. Danninger, The Effect of Boron Liquid Phase Sintering on Properties of Ni-, Mo- and Cr-Alloyed Structural Steels, *Int. J. Mater. Process. Technol.*, 2003, **141–143**, p 910–915
5. A. Lal, J. Liu, R.G. Iacocca, and R.M. German, Precision in Supersolidus Liquid Phase Sintering of Prealloyed Powders, *Metall. Mater. Trans. A*, 1999, **30**, p 2209–2220
6. M. Sarasola, T. Gomez-Acebo, and F. Catro, Liquid Generation During Sintering of Fe-3.5%Mo Powder Compacts with Elemental Boron Additions, *Acta Mater.*, 2004, **52**, p 4615–4622
7. R.M. German, *Liquid Phase Sintering*, 2nd ed., Plenum Press, New York, 1985, p 43–99
8. T.B. Sercombe, Sintering of Freeformed Maraging Steel with Boron Additions, *Mater. Sci. Eng. A*, 2003, **363**, p 242–252
9. T.B. Massalski, *Binary Phase Diagrams*, Vol I and II, ASM International, Materials Park, OH, 1986, p 482, 1273
10. J. Kazior, A. Molinari, C. Janczur, and T. Pieczonka, Microstructural Characterization and Properties of Thermochemically Treated Iron-Based Alloys, *Surf. Coat. Technol.*, 2000, **125**, p 1–8
11. A. Bautista, C. Moral, G. Blanco, and F. Velasco, Mechanical and Oxidation Properties of High Density Sintered Duplex Stainless Steels Obtained from Mix of Water and Gas Atomised Powders, *Powder Metall.*, 2006, **49**(3), p 265–273
12. F. Akhtar, Sintering Behavior of Elemental Powders with FeB Addition in the Composition of Martensitic Stainless Steel, *J. Mater. Eng. Perform.*, 2007, **16**, p 726–729
13. ISO 3369, "Impermeable Sintered Metal Materials and Hardmetals—Determination of Density," International Organization for Standardization, 1995
14. Z. Xiu, A. Salwén, X. Qin, F. He, and X. Sun, Sintering Behaviour of Iron-Molybdenum Steels with the Addition of Fe-B-C Master Alloy Powders, *Powder Metall.*, 2003, **46**(2), p 171–174
15. R.W.K. Honeycomb and H.K.D.H. Bhadeshia, *Steels, Microstructure and Properties, Metallurgy and Materials Science*, 2nd ed., Edward Arnold Butterworth Heinemann, London, England, 1995, p 60–82
16. H.I. Bakan, D. Heaney, and R.M. German, Effect of Nickel Boride and Boron Additions on Sintering Characteristics of Injection Moulded 316L Powder Using Water Soluble Binder System, *Powder Metall.*, 2001, **44**(3), p 235–242
17. J.A. Cabral-Miramontes, J.D.O. Barceinas-Sánchez, L. Vélez-Jacobo, A. Martínez-Villafañe, and J.G. Chacón-Nava, Efecto del boro en la sinterización de un acero inoxidable ferrítico (Effect of Boron on Sintering of a Ferritic Stainless Steel), *Rev. Metal. Madrid*, **44**(6), 2008, p 493–502
18. J. Karwan-Baczewska and M. Rosso, Effect of Boron on Microstructural and Mechanical Properties of PM Sintered and Nitrided Steels, *Powder Metall.*, 2001, **44**(3), p 221–227
19. N. Fujita, H.K.D.H. Bhadeshia, and M. Kikuchi, Precipitation Sequence in Niobium-Alloyed Ferritic Stainless Steel, *Model Simul. Mater. Sci. Eng.*, 2004, **12**, p 273–284
20. I.F. Machado and A.F. Padilha, The Occurrence of Laves Phase in Fe-15%Cr-15%Ni Austenitic Stainless Steels Containing Niobium, *Acta Microsc.*, 2003, **12**(1), p 111–114
21. D. Krecar, V. Vassileva, H. Danninger, and H. Hutter, Characterization of the Distribution of the Sintering Activator Boron in Powder Metallurgical Steels with SIMS, *Anal. Bioanal. Chem.*, 2004, **379**, p 605–609